https://doi.org/10.5194/mr-2021-25
Preprint. Discussion started: 15 March 2021


Open Access MAGNETIC RESONANCE Discussions

# Solid-State $^{1}$H Spin Polarimetry by $^{13}CH_3$ Nuclear Magnetic Resonance

Stuart J. Elliott[1,2], Quentin Stern[1] and Sami Jannin[1]

[1]Centre de Résonance Magnétique Nucléaire à Très Hauts Champs - FRE 2034 Université de Lyon / CNRS / Université Claude Bernard Lyon 1 / ENS de Lyon, 5 Rue de la Doua, 69100 Villeurbanne, France
[2]Department of Chemistry, University of Liverpool, Liverpool L69 7ZD, United Kingdom

*Correspondence to*: Stuart J. Elliott (stuart-james.elliott@univ-lyon1.fr)

**Abstract.** Dissolution-dynamic nuclear polarization is emerging as a promising means to prepare proton polarizations approaching unity. At present, $^{1}$H polarization quantification remains fastidious due to the requirement of measuring thermal equilibrium signals. Lineshape polarimetry of solid-state nuclear magnetic resonance spectra is used to determine a number of useful properties regarding the spin system under investigation. In the case of highly polarized nuclear spins, such as those prepared under the conditions of dissolution-dynamic nuclear polarization experiments, the absolute polarization of a particular isotopic species within the sample can be directly inferred from the characteristics of the corresponding resonance lineshape. In situations where direct measurements of polarization are complicated by deleterious phenomena, indirect estimates of polarization using coupled heteronuclear spins prove informative. We present a simple analysis of the $^{13}$C spectral lineshape asymmetry of [2-$^{13}$C]sodium acetate based on relative peak intensities, which can be used to indirectly evaluate the proton polarization of the methyl group moiety, and very likely the entire sample in the case of rapid and homogeneous $^{1}$H-$^{1}$H spin diffusion. $^{1}$H polarizations greater than ~10-25% (depending on the sign of the microwave irradiation) were found to be linearly proportional to the $^{13}$C peak asymmetry, which responds differently to positive or negative microwave irradiation. These results suggest that, as a dopant, [2-$^{13}$C]sodium acetate could be used to indirectly gauge $^{1}$H polarizations in standard sample formulations, which is potentially advantageous for: samples polarized in commercial dissolution-dynamic nuclear polarization devices that lack $^{1}$H radiofrequency hardware, measurements which are deleteriously influenced by radiation damping or complicated by the presence of large background signals, and situations where the acquisition of a thermal equilibrium spectrum is not feasible.

## 1 Introduction

Classical nuclear magnetic resonance (NMR) experiments produce inherently weak signals. The severely limiting low intrinsic sensitivity of the technique can be enhanced by up to four orders of magnitude by employing a wide range of routinely used hyperpolarization methodologies (Ardenkjær-Larsen et al., 2003; Hirsch et al., 2015; Hirsch et al., 2015; Ardenkjær-Larsen et al., 2016; Dale and Wedge, 2016; Barskiy et al, 2017; Salnikov et al, 2017; Ardenkjær-Larsen et al., 2018; Kovtunov et al., 2018; Meier 2018; Jannin and Kurzbach, 2018; Ardenkjær-Larsen, 2019). The significantly boosted NMR signal intensities from metabolites hyperpolarized by implementing a dissolution-dynamic nuclear polarization (*d*DNP) approach have been put to use in the clinical diagnostics of cancer in human patients (Day et al, 2007; Brindle et al, 2011; Nelson et al, 2013).

To hyperpolarize nuclear spins via the *d*DNP approach, the spin system of interest is co-frozen in a mixture of aqueous solvents and glassing agents with a carefully chosen paramagnetic radical species (Jannin et al, 2019). The *d*DNP-compatible solution is subsequently frozen at liquid helium temperatures, where the solvent matrix forms a glass, inside a magnetic field and is irradiated with slightly non-resonant microwave irradiation, which transfers the high electron spin polarization to the nuclear spins of interest (Kundu et al, 2019).

Hyperpolarization of methyl group moieties by *d*DNP has led to some unusual effects including the generation of long-lived spin order, which is revealed in the liquid-state upon dissolution of the material from cryogenic conditions (Meier et al, 2013; Roy et al, 2015; Dumez et al, 2017; Elliott et al, 2018). Solid-state NMR polarimetry of highly polarized nuclear spin-1/2 pairs has previously been utilized to infer the sample polarization level and, in suitable cases, the quantity of long-lived spin order established

https://doi.org/10.5194/mr-2021-25
Preprint. Discussion started: 15 March 2021


Open Access MAGNETIC RESONANCE Discussions

(Meier et al, 2013; Roy et al, 2015; Dumez et al, 2017; Elliott et al, 2018; Waugh et al, 1987; Kuhns et al, 1989; Marohn et al, 1995; Kuzma et al, 2013; Mammoli et al, 2015; Willmering et al, 2017; Aghelnejad et al, 2020). Until now, the solid-state NMR spectra of strongly polarized methyl groups have not shown any significant features which may be used for a clear lineshape analysis.

In this Communication, we propose that the $^{13}$C NMR lineshape of [2-$^{13}$C]sodium acetate can be used to indirectly quantify the $^{1}$H polarization of the methyl group spins. Furthermore, since $^{1}$H-$^{1}$H spin diffusion rapidly achieves a homogeneous proton polarization across the entire sample, the $^{1}$H polarization level of the whole sample is therefore likely to be reflected by the $^{1}$H polarization of the methyl group moiety. We analyze the asymmetry of the experimental $^{13}$C NMR spectra acquired for different $^{1}$H polarizations, and herein present a straightforward approach to indirectly quantify the $^{1}$H polarization based on the relative intensities of the $^{13}$C peaks. The $^{13}$C peak asymmetry was found to behave differently under positive or negative microwave frequencies, and $^{1}$H polarizations (exceeding ~10-25%) were observed to decrease linearly with increasing $^{13}$C peak asymmetries (depending on the sign of the microwave irradiation).

## 2. Methods

### 2.1. Sample Preparation

A solution of 3 M [2-$^{13}$C]sodium acetate in the glass-forming mixture $H_2O/D_2O$/glycerol-$d_8$ (1/3/6 *v*/*v*/*v*) was doped with 50 mM TEMPOL radical (all compounds purchased from *Sigma Aldrich*) and sonicated for ~10 minutes. This sample is referred to as **I** from here onwards. Paramagnetic TEMPOL radicals were chosen to most efficiently polarize $^{1}$H spins under our *d*DNP conditions.

### 2.2. Sample Freezing

A 100 $\mu$L volume of **I** was pipetted into a Kel-F sample cup and inserted into a 7.05 T prototype *Bruker Biospin* polarizer equipped with a specialized *d*DNP probe, including a background-free radiofrequency (*rf*) coil insert (Ceillier et al, 2021), running *TopSpin 3.5* software. The sample temperature was reduced to 1.2 K by submerging the sample in liquid helium and reducing the pressure of the variable temperature insert (VTI) towards ~0.7 mbar.

### 2.3. Dynamic Nuclear Polarization

The 100 $\mu$L sample of **I** was polarized by applying microwave irradiation at $f_{\mu w}$ = 197.616 GHz (positive lobe of the DNP enhancement profile) or $f_{\mu w}$ = 198.192 GHz (negative lobe of the DNP enhancement profile) with triangular frequency modulation (Bornet et al, 2014) of amplitude $\Delta f_{\mu w}$ = ± 136 MHz or $\Delta f_{\mu w}$ = ± 112 MHz, respectively, and rate $f_{mod}$ = 0.5 kHz at a power of ca. $P_{\mu w}$ = 125 mW at the output of the microwave source and ca. $P_{\mu w}$ = 30 mW reaching the DNP cavity (evaluated by monitoring the helium bath pressure), which were optimized prior to commencing experiments to achieve the best possible level of $^{1}$H polarization.

### 2.4. Polarization Build-Ups

In order to monitor $^{13}$C NMR spectral lineshapes with satisfactory signal-to-noise ratios (SNRs), $^{13}$C polarization must first be built-up by using a succession of optimized cross-polarization (CP) contact *rf*-pulses. Then, to observe changes in the lineshape of $^{13}$C NMR spectra acquired as the $^{1}$H polarization builds-up from thermal to DNP equilibria, we employed a series of $^{1}$H crusher *rf*-pulses followed by microwave activation and small *rf*-pulse flip-angle $^{13}$C NMR signal detection, as shown by the *rf*-pulse sequence

https://doi.org/10.5194/mr-2021-25
Preprint. Discussion started: 15 March 2021


Open Access MAGNETIC RESONANCE Discussions

in Figure 1. The build-up of $^{13}C$ polarization throughout the microwave irradiation period for sample **I** was tracked by engaging the following experimental procedure:

(*i*) A crusher sequence of 90° *rf*-pulses with alternating phases separated by a short delay (typ. 11 ms) repeated *n* times (typ. *n* = 50) kills residual magnetization on both *rf*-channels;

(*ii*) The microwave source becomes active and $^{1}H$ polarization builds-up;

(*iii*) The $^{13}C$ Zeeman magnetization trajectory is minimally perturbed by the application of a small flip-angle *rf*-pulse (typ. $\beta$ = 3.5°) with a short acquisition period (typ. $t_{FID}$ = 1 ms) used for detection;

(*iv*) $^{1}H$ DNP builds-up during a time $t^1_{DNP}$ (typ. $t^1_{DNP}$ = 30 s);

(*v*) Stages *iii*-*iv* are cycled *m* times (typ. *m* = 6) in order to monitor the evolution of the $^{13}C$ polarization (between CP steps);

(*vi*) The microwave source is gated and a delay of duration $t_G$ = 0.5 s occurs, see Section 2.5, thus permitting the electron spins to relax to their highly polarized thermal equilibrium state before the next CP step (Bornet et al, 2016);

(*vii*) Two synchronized adiabatic half-passages (AHPs) simultaneously produce transverse magnetization for all pulsed spin species;

(*viii*) The nuclear magnetization is subsequently spin-locked on both *rf*-channels (typically by a high power *rf*-pulse with a nutation frequency on the order of 15 kHz and a duration between 1-10 ms), and $^{1}H \rightarrow ^{13}C$ polarization transfer occurs (Bornet et al, 2016);

(*ix*) A second pair of harmonized AHPs (operating with reverse chronology) restores Zeeman magnetization on each *rf*-channel;

(*x*) Stages *ii*-*ix* are repeated in *L* units (typ. *L* = 8) to periodically transfer $^{1}H$ Zeeman polarization to $^{13}C$ nuclear spins;

(*xi*) A second crusher sequence of 90° *rf*-pulses with alternating phases separated by a short delay (typ. 11 ms) repeated *n* times (typ. *n* = 50) kills residual magnetization on the $^{1}H$ *rf*-channel only;

(*xii*) The microwave source reactivates;

(*xiii*) The $^{13}C$ Zeeman magnetization trajectory is minimally perturbed by the application of a small flip-angle *rf*-pulse (typ. $\beta$ = 3.5°) with a short acquisition period (typ. $t_{FID}$ = 1 ms) used for detection;

(*xiv*) $^{1}H$ DNP builds-up during a time $t^2_{DNP}$ (typ. $t^2_{DNP}$ = 5 s);

(*xv*) Stages *xiii*-x*iv* are cycled *p* times (typ. *p* = 80) to monitor the evolution of the $^{13}C$ NMR spectra as a function of the $^{1}H$ polarization build-up with sufficient SNR.

Further details regarding multiple-contact CP *rf*-pulse sequence operation are given elsewhere (Bornet et al, 2016).

Since it is unlikely that the $^{13}C$ NMR lineshape of **I** is significantly influenced by the $^{13}C$ polarization, we can afford not to diminish the $^{13}C$ NMR signal intensity by a sequence of $^{13}C$ crusher *rf*-pulses on the $^{13}C$ *rf*-channel at stage *xi* in order to maintain high SNRs. The small *rf*-pulse flip angles are necessary in order to preserve the $^{1}H$ and $^{13}C$ polarizations throughout the course of the build-up experiment.

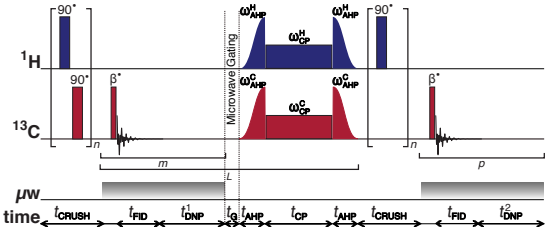


**Figure 1: Schematic representation of the *rf*-pulse sequence used to accrue $^{13}C$ polarizations, and monitor $^{13}C$ lineshapes as a function of the $^{1}H$ polarization. The experiments used the following key parameters, chosen to maximize the efficiency of the *rf*-pulse sequence: *n* = 50; $\beta$ = 3.5°; *m* = 6; $t^1_{DNP}$ = 30 s; *L* = 8; $t_G$ = 0.5 s; *p* = 80; and $t^2_{DNP}$ = 5 s. AHP = adiabatic half-passage. AHP sweep width = 100 kHz. The $\pi/2$ crusher *rf*-pulses used an empirically**

https://doi.org/10.5194/mr-2021-25
Preprint. Discussion started: 15 March 2021


Open Access MAGNETIC RESONANCE Discussions

**optimized thirteen-step phase cycle to remove residual magnetization at the beginning of each experiment: {0, π/18, 5π/18, π/2, 4π/9, 5π/18, 8π/9, π, 10π/9, 13π/9, π/18, 5π/3, 35π/18}. The resonance offset was placed at the most intense peak of the $^{1}$H and $^{13}$C NMR spectra.**

### 2.5. Microwave Gating

Microwave gating was employed shortly before and during CP experiments to allow the electron spin ensemble to return to a highly polarized state, which happens on the timescale of the longitudinal electron relaxation time (typ. $T_{1e}$ = 100 ms with $P_e$ = 99.93% under our *d*DNP conditions) (Bornet et al, 2016). Microwave gating hence provides a way to strongly attenuate paramagnetic relaxation, and consequently the $^{1}$H and $^{13}$C $T_{1\rho}$ relaxation time constants in the presence of an *rf*-field are extended by orders of magnitude. This allows spin-locking *rf*-pulses to be much longer, which significantly increases the efficiency of nuclear polarization transfer.

## 3. Results

### 3.1. $^{13}$C CP Build-Ups and Decays

The CP build-up curves for the $^{13}$C polarizations $P_C$ of **I** as a function of the $^{1}$H DNP time $t_{DNP}$ for both positive and negative microwave irradiation are shown in Figure 2. The $^{13}$C polarizations $P_C$ were accrued by employing the *rf*-pulse sequence shown in Figure 1. For sample **I**, the $^{13}$C polarizations $P_C$ ultimately reached $P_C \simeq 40.6\%$ and $P_C \simeq -46.8\%$ after numerous CP transfers and 24 minutes of positive and negative microwave irradiation, respectively. The achieved levels of $^{13}$C polarization $P_C$ are lower than those previously reported in the literature (Bornet et al, 2016), but were not further optimized since only the $^{13}$C NMR lineshape was of interest in this study as a probe for absolute $^{1}$H polarization.

After this point, *i.e.* beyond the dashed line at $^{1}$H DNP time = 24 mins, a slow and partial decay in the $^{13}$C NMR signal intensity towards a pseudo-equillibrium is observed, see Figure 2. This is not a problem in itself as the $^{13}$C NMR signal remains sufficiently intense as to allow clear measurement of the $^{13}$C NMR lineshape with high accuracy.

This decay of $^{13}$C polarization during the $^{1}$H DNP build-up interval $t^2_{DNP}$ is a combination of two factors: (*i*) the microwaves are active and hence polarization is diminishing towards the low DNP equilibrium of the $^{13}$C nuclear spins with TEMPO(L) as the polarizing agent; and (*ii*) the $^{13}$C nuclear spins are being actively pulsed, although minimally, every 5 s, which leads to an accumulative loss of $^{13}$C NMR signal intensity over many minutes.

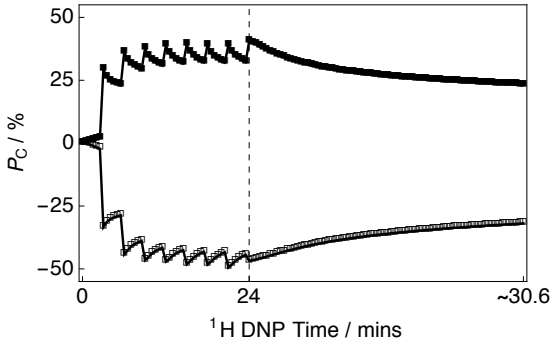


**Figure 2: Experimental $^{13}$C polarization $P_C$ CP build-up curves and subsequent $^{13}$C signal decays for I as a function of $^{1}$H DNP time acquired at 7.05 T ($^{1}$H nuclear Larmor frequency = 300.13 MHz, $^{13}$C nuclear Larmor frequency = 75.47 MHz) and 1.2 K with a single transient per data point. The presented data were acquired by using the *rf*-pulse sequence depicted in Figure 1. Black filled squares: Positive microwave irradiation; Black empty squares:**

https://doi.org/10.5194/mr-2021-25
Preprint. Discussion started: 15 March 2021


Open Access MAGNETIC RESONANCE Discussions

**Negative microwave irradiation. The dashed line denotes the $^{1}$H DNP time at which the $^{1}$H NMR signal was destroyed by a second series of crusher *rf*-pulses (as shown by the *rf*-pulse sequence depicted in Figure 1).**

### 3.2. $^{13}$C NMR Spectra

Figure 3 shows the relevant part of the experimental $^{13}$C NMR spectra for sample **I** acquired with a small flip angle *rf*-pulse ($\beta$ = 3.5°) at two different $^{1}$H DNP times. The $^{13}$C NMR spectra in Figure 3 were acquired by using the *rf*-pulse sequence shown in Figure 1. The initial $^{13}$C NMR spectra (acquired at 24 mins) are single peaks which are relatively symmetrical and have no obvious defining features, see Figures 3a and 3c. These spectra correspond to low levels of $^{1}$H polarization ($|P_H| \simeq 0\%$).

However, the $^{13}$C NMR spectra become more complicated and gain sharper spectral features at extended $^{1}$H DNP times, see Figures 3b and 3d. These spectra correspond to much higher levels of $^{1}$H polarization ($|P_H| \gtrsim 60\%$), see Figure 4. At ~30.6 mins, the $^{13}$C NMR spectra are comprised of two separate resonances with differing NMR signal intensities. It is interesting to note that the $^{13}$C NMR spectra acquired in the cases of positive (Figure 3b) and negative (Figure 3d) microwave irradiation are not mirror images of each other at long $^{1}$H DNP times.

The difference in $^{13}$C NMR signal integrals for positive and negative microwave irradiation is associated with the $^{1}$H polarization build-ups and the performance efficiency of the multiple-contact CP *rf*-pulses, see the Supplement. However, this is inconsequential for the current study since sufficient SNRs on the order of ~965 and ~1244 were achieved for the cases of positive and negative microwave irradiation, respectively.

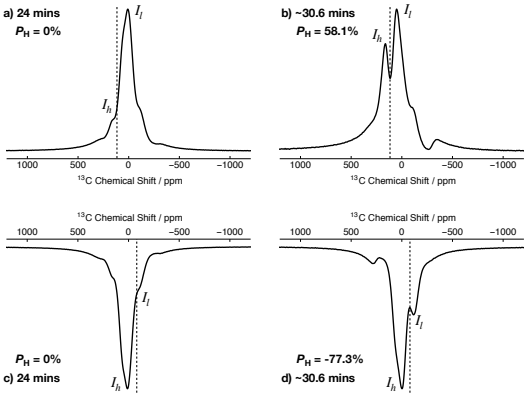


**Figure 3: Relevant portions of the experimental $^{13}$C NMR spectra belonging to the $^{13}$C-labelled methyl ($^{13}CH_3$) group of I acquired at 7.05 T ($^{1}$H nuclear Larmor frequency = 300.13 MHz, $^{13}$C nuclear Larmor frequency = 75.47 MHz) and 1.2 K with a single transient (*rf*-pulse flip angle = 3.5°) at two different $^{1}$H DNP times. The labels indicate the $^{1}$H DNP times at which the spectra were recorded. The timings coincide with those shown in Figure 2. The $^{13}$C NMR spectra were acquired by using the *rf*-pulse sequence depicted in Figure 1. (a,b) Positive microwave irradiation; and (c,d) Negative microwave irradiation. $I_h$ and $I_l$ indicate the intensities of the high and low frequency $^{13}$C NMR peaks, respectively. The vertical dashed lines separate the $^{13}$C NMR peaks $I_h$ and $I_l$, and are located at +64.8ppm (positive microwave irradiation) and -113.9ppm (negative microwave irradiation). All $^{13}$C NMR spectra have been scaled to yield the same maximum intensity.**

### 3.3. $^{13}$C NMR Peak Asymmetry vs. $^{1}$H Polarization

The DNP build-up curve for the $^{1}$H polarization $P_H$ of **I** as a function of the $^{1}$H DNP time for positive microwave irradiation is shown in Figure 4. More details regarding how to acquire such build-up curves are given in the following reference (Bornet et al, 2016). The $^{1}$H polarization build-up curve was found to have a stretched exponential behaviour, and the experimental data are well

https://doi.org/10.5194/mr-2021-25
Preprint. Discussion started: 15 March 2021


Open Access MAGNETIC RESONANCE Discussions

fitted with a stretched exponential function using a sole $^1$H DNP build-up time constant denoted $\tau^+_{\mathrm{DNP}}$. Stretched exponential function: A(1-exp{-($t/\tau^+_{\mathrm{DNP}}$)$^{\beta}$}), where A is a constant, $\tau^+_{DNP}$ is the $^1$H DNP build-up time constant extracted from the above fitting procedure and $\beta$ is the breadth of the distribution of $^1$H DNP build-up time constants. The mean $^1$H DNP build-up time constant $\langle\tau^+_{DNP}\rangle$ is calculated as follows: $\langle\tau^+_{DNP}\rangle = \tau^+_{DNP}\Gamma(1/\beta)/\beta$, where $\Gamma(1/\beta)$ is the gamma function. A similar $^1$H polarization build-up curve for the case of negative microwave irradiation, with parameters $\tau^-_{\mathrm{DNP}}$ and $\langle\tau^-_{\mathrm{DNP}}\rangle$, is shown in the Supplement.

Sample **I** polarizes to $P_{\mathrm{H}} \simeq$ -77.3% (at $^1$H DNP time $\simeq$ 30.6 mins) by employing negative microwave irradiation with a $^1$H DNP build-up time constant of $\langle\tau^-_{\mathrm{DNP}}\rangle$ = 122.0 ± 0.4 s. A reduced $^1$H polarization of $P_{\mathrm{H}} \simeq$ 58.1% was reached (at $^1$H DNP time $\simeq$ 30.6 mins) by using positive microwave irradiation. The $^1$H DNP build-up time constant was much shorter in this case: $\langle\tau^+_{\mathrm{DNP}}\rangle$ = 80.2 ± 0.3 s.

Figure 4 also displays the $^{13}$C NMR peak asymmetry $A_{\mathrm{sym}}$ for sample **I** as a function of the $^1$H DNP time. The $^{13}$C NMR peak asymmetry $A_{\mathrm{sym}}$ is defined as:

$$A_{\mathrm{sym}} = \mathrm{Sign}(P_{\mathrm{C}})\frac{I_l - I_h}{I_l + I_h}, \quad (1)$$

where $I_h$ and $I_l$ are the maximum intensities of the high and low frequency $^{13}$C NMR peaks, respectively, see Figure 3. $I_h$ and $I_l$ are extracted from the $^{13}$C NMR spectra in Figure 3, and those similar to it, by searching for the most intense data point either side of the vertical dashed line. The frequency of the dashed line corresponds to the minimum between the two peaks at high levels of $^1$H polarization $P_{\mathrm{H}}$, see Figures 3b and 3d. This coincides with small spectral contributions at low levels of $^1$H polarization $P_{\mathrm{H}}$, see Figures 3a and 3c.

Figure 4 indicates that at longer $^1$H DNP times, where the $^1$H polarization $P_{\mathrm{H}}$ is higher, the peak intensities become more equal. This is opposite to the case of strongly polarized water (Mammoli et al, 2015), and other systems (Aghelnejad et al, 2020), where the peak intensities become more unequal with increasing $^1$H polarization $P_{\mathrm{H}}$. A similar curve for the case of negative microwave irradiation is shown in the Supplement. It should be noted that the curve profiles and final values of $A_{\mathrm{sym}}$ are not mirror images of each other. This is also reflected in the $^{13}$C NMR spectra acquired at ~30.6 mins, see Figure 3. The rate of change in the value of $A_{\mathrm{sym}}$ during the first ~100 s of Figure 4 indicates a more rapid change in the $^1$H polarization $P_{\mathrm{H}}$. This also coincides with the starkest changes in $^{13}$C NMR lineshape, see the Supplement.

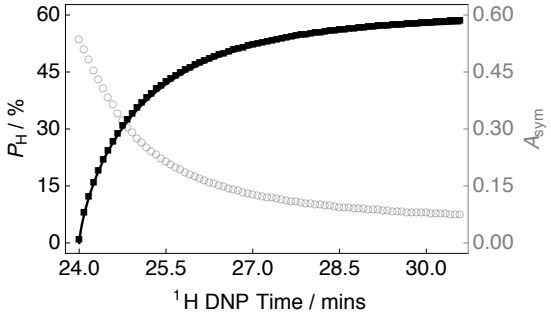


**Figure 4: Experimental $^1$H polarization $P_{\mathrm{H}}$ DNP build-up curve (black filled squares and left-hand axis) and $^{13}$C NMR peak asymmetry $A_{\mathrm{sym}}$ (grey empty circles and right-hand axis) for I as a function of the $^1$H DNP time acquired at 7.05 T ($^1$H nuclear Larmor frequency = 300.13 MHz, $^{13}$C nuclear Larmor frequency = 75.47 MHz) and 1.2 K with a single transient per data point for the case of positive microwave irradiation. The timings coincide with those shown in Figure 2. The black solid line indicates the best fit of experimental data points for the $^1$H polarization $P_{\mathrm{H}}$ DNP build-up curve, and has the corresponding fitting function: A(1-exp{-($t/$\tau^+_{\mathrm{DNP}}$)$^{\beta}$}). Mean $^1$H DNP build-up time constant: $\langle\tau^+_{\mathrm{DNP}}\rangle$ = 80.2 ± 0.3 s.**

https://doi.org/10.5194/mr-2021-25
Preprint. Discussion started: 15 March 2021


Open Access MAGNETIC RESONANCE Discussions

The $^{13}$C NMR peak asymmetry $A_{sym}$ for sample **I** as a function of the $^{1}$H polarization $P_H$ is shown in Figure 5. The magnitude of the $^{1}$H polarization $|P_H|$ increases linearly with a decreasing $^{13}$C NMR peak asymmetry for $A_{sym} < 0.5$ where $I_1/I_2 > 3$.

The data were fitted with relationships of the kind: $P_H(|A_{sym}|) = m|A_{sym}| + \eta$, where $P_H(|A_{sym}|)$ is the $^{1}$H polarization as a function of the $^{13}$C peak asymmetry parameter $A_{sym}$, $m$ is the slope of the linear fit and $\eta$ is a fitting constant. The slopes of the straight line fits to the experimental data over the range of $^{13}$C peak asymmetries $A_{sym}$ shown in Figure 5 are given in the caption. The slope for positive microwave irradiation in Figure 5 is a factor of ~1.87 less steep than for the case of negative microwave irradiation. This result implies that the $^{13}$C peak asymmetry $A_{sym}$ of **I** is more sensitive to negative microwave irradiation since sample **I** polarizes to a greater extent under this choice of microwave irradiation frequency. The divergence in $^{13}$C peak asymmetries $A_{sym}$ under positive and negative microwave irradiation is also evident in the $^{13}$C NMR spectra, see Figure 3 and the Supplement.

The experimental data deviate, severely in the case of negative microwave irradiation, from the linear fits at $^{13}$C asymmetry parameters $A_{sym} > 0.5$. This is likely associated with the $^{13}$C NMR spectra at lower levels of $^{1}$H polarization having lineshapes with a reduced number of features, *i.e.* peaks, and more generally speaking, especially in the case of negative microwave irradiation, because the $^{13}$C NMR lineshape changes less dramatically as a function of the $^{1}$H polarization for $|P_H| \lesssim 25\%$. Clearly, at low levels of $^{1}$H polarization $P_H$ the lower intensity resonance is polluted by the more intense peak, and as such; the above procedure (described by Equation 1) rapidly fails.

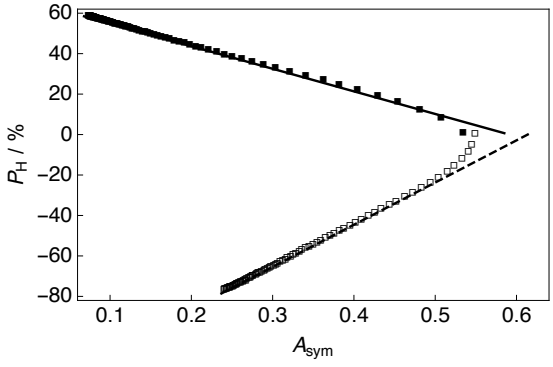


**Figure 5: Experimental $^{1}$H polarizations $P_H$ for I as a function of the $^{13}$C NMR peak asymmetry $A_{sym}$ acquired at 7.05 T ($^{1}$H nuclear Larmor frequency = 300.13 MHz, $^{13}$C nuclear Larmor frequency = 75.47 MHz) and 1.2 K with a single transient per data point. Black filled squares: Positive microwave irradiation; Black empty squares: Negative microwave irradiation. The data were fitted with a straight line function including a non-zero intercept: $P_H(|A_{sym}|) = m|A_{sym}| + \eta$. Best fit values: Positive microwave irradiation (black solid line): $m$ = -111.7%; $\eta$ = 66.0%; Negative microwave irradiation (black dashed line): $m$ = 208.5%; $\eta$ = -128.0%. Data points at $A_{sym} > 0.5$ were neglected from the fit.**

## 4. Discussion

As discussed in Section 3.3 above, the asymmetry in the intensity of the $^{13}$C NMR spectral components $A_{sym}$ indirectly provides the level of $^{1}$H polarization $P_H$, see Figure 5. It should be noted that the linearity of the slopes shown in Figure 5 are likely to be influenced by the capabilities of the *rf*-probe, such as the *rf*-pulse homogeneity, and it is therefore recommended that (if possible) users implement similar measurements on their own experimental setups, rather than simply reusing the gradient values presented here. Since the two fits to the experimental data in Figure 5 have different slopes, prior knowledge of the sign of the microwave irradiation must also be determined prior to experiments.

To the approach's detriment, once the $^{13}$C NMR peak asymmetry $A_{sym}$ exceeds ~0.5 the $^{1}$H polarization $P_H$ deviates from a linear trend, dropping towards zero rapidly (with little change in the $^{13}$C asymmetry parameter $A_{sym}$) since the $^{13}$C NMR spectra

https://doi.org/10.5194/mr-2021-25
Preprint. Discussion started: 15 March 2021


Open Access MAGNETIC RESONANCE Discussions

lose any pronounced lineshape features, see Figure 3 and the Supplement. This corresponds to $^{1}$H polarizations in the range of $|P_H| \simeq$ 10-25% (microwave frequency sign dependent), such as those typically accrued by $^{1}$H DNP build-up experiments at liquid helium temperatures of 3.8-4.2 K. These results indicate that the $^{13}$C peak asymmetry $A_{sym}$ cannot be used to infer $^{1}$H polarizations $P_H$ accurately at elevated temperatures. Furthermore, the presence of methyl group rotation at temperatures above 1.2 K could also be detrimental to the presented approach (Latanowicz, 2005).

It is unlikely that a uniform spin temperature between the $^{1}$H and $^{13}$C nuclear spin reservoirs is reached at any time during the experiment presented in Figure 1, but as long as a uniform spin temperature is achieved within each independent nuclear spin reservoir then the methodology presented above holds. One possible contribution to the deviation in $^{13}$C NMR peak asymmetry $A_{sym}$ from a linear trend at low levels of the $^{1}$H polarization $P_H$ is the presence of strong polarization gradients or highly polarized clusters of nuclear spins located within specific radii of the electron spins within the sample at short $^{1}$H DNP times, which would lead to a non-uniform spin temperature. This contribution is expected to be minor.

Furthermore, in Figure 5 it is noticeable that the $^{13}$C NMR peak asymmetry $A_{sym}$ is not identical near $|P_H| = 0$. This shows that the $^{13}$C polarization, and sign thereof, could have a small impact on the $^{13}$C NMR peak asymmetry $A_{sym}$. This feature is also likely related to the extraction of peak intensities from the somewhat featureless $^{13}$C NMR lineshapes at low levels of $^{1}$H polarization $P_H$, see Figures 3a and 3c. The slight discrepancy in lineshape between these two spectra may additionally be related to residual $^{1}$H polarization, of opposite sign, which may not have been completely destroyed by the second series of crusher *rf*-pulses implemented on the $^{1}$H *rf*-channel of our spectrometer.

The slope of the curves presented in Figure 5 is likely to depend to a small degree on the solvent constituents. In the case of sample **I**, the glycerol-$d_8$ present in the *d*DNP glassing matrix yields an approximate $^{13}$C concentration of ~410 mM at natural abundance. This is ~14% of the total $^{13}$C NMR signal, which could go some way to explaining why the $^{13}$C NMR spectra are not mirror images of one and other under positive and negative microwave irradiation at long proton DNP time durations, see Figures 3a and 3c. This contribution also possibly impacts the $^{13}$C NMR peak intensities, their ratios and the value of $A_{sym}$.

The NMR spectra presented in Figure 3 were acquired for the cases of high $^{13}$C SNRs, the largest of which is ca. ~1250. In the event that CP cannot be efficiently implemented and the acquired $^{13}$C NMR signal is weak, we anticipate that the method is robust with respect to a few kilohertz of Lorentzian line broadening, which can be used to improve the experimental SNR. The intensities of the $^{13}$C NMR peaks in Figure 3 are, however, likely to be sensitive to changes in phase, and this should therefore be taken into account before comparing experimental results to any calibration curves similar to those presented in Figure 5. It is also possible that additional phase corrections may help the trends shown in Figure 5 become linear at values of $A_{sym} > 0.5$.

The results of this study suggest that $^{13}$C-labelled molecules which display distinctly asymmetric solid-state $^{13}$C NMR spectra, such as [1-$^{13}$C]sodium formate and other $^{13}CH_3$ methyl group moiety bearing molecular candidates, could also be used as indirect $^{1}$H polarization meters. To effectively polarize both $^{1}$H and $^{13}$C nuclear spins, future experiments could use a tailored mixture of radical species, in certain cases. The presented analysis could be further improved by considering Voigt fits of the complicated $^{13}$C NMR spectra, but this route would lead us away from our simple pedagogical approach.

## 5 Conclusions

We have demonstrated that $^{13}$C NMR lineshape polarimetry of [2-$^{13}$C]sodium acetate can be implemented to indirectly infer the $^{1}$H polarization of the $^{13}CH_3$ group nuclear spins, and potentially the whole sample if the constituents of which are sufficiently homogeneously mixed. An easy to implement protocol based on relative peak intensities was employed and found a linear relationship of the $^{13}$C peak asymmetry with increasing $^{1}$H polarizations surpassing ~10-25% (depending on the sign of the microwave frequency), with different $^{13}$C NMR lineshapes for positive and negative microwave irradiation.

This approach is complementary to traditional methods of measuring $^{1}$H polarization, in suitable circumstances, and could be useful in situations where measurements of $^{1}$H polarization prove difficult, *e.g.* due to radiation damping (Mao and Ye, 1997),

https://doi.org/10.5194/mr-2021-25
Preprint. Discussion started: 15 March 2021


Open Access MAGNETIC RESONANCE Discussions

which can also likely impact the slope of the fits shown in Figure 5. Other appropriate cases for potential implementation include: (*i*) the lack of a $^{1}$H *rf*-coil; (*ii*) the presence of large background signals; and (*iii*) the absence of a thermal equilibrium spectrum. The approach presented here works well for traditional *d*DNP-compatible sample formulations but future studies employing fully deuterated *d*DNP solutions could provide $^{13}$C NMR lineshapes with more distinct features, and also reveal information regarding solid-state methyl group AE population imbalances at low temperatures (Meier et al, 2013; Roy et al, 2015; Dumez et al, 2017).

**Acknowledgements**

The authors gratefully acknowledge *Bruker Biospin* for providing the prototype *d*DNP polarizer, and particularly Dmitry Eshchenko, Roberto Melzi, Marc Rossire, Marco Sacher and James Kempf for scientific and technical support. The authors additionally acknowledge Catherine Jose and Christophe Pages for use of the ISA Prototype Service, Stéphane Martinez of the UCBL mechanical workshop for machining parts of the experimental apparatus, Aurélien Bornet for preliminary works and Christian Bengs for useful discussions.

**Financial Support**

This research was supported by ENS-Lyon, the French CNRS, Lyon 1 University, the European Research Council under the European Union's Horizon 2020 research and innovation program (ERC Grant Agreements No. 714519 / HP4all and Marie Skłodowska-Curie Grant Agreement No. 766402 / ZULF).

**Author Contributions**

SJE conceived the idea, performed experiments, processed the data and wrote the manuscript, QC assisted with experiments and data processing, and provided useful advice, and SJ provided informative guidance and supportive feedback, and contributed to the manuscript.

**Data Availability**

Experimental data are available upon request from the corresponding author.

**Competing Interests**

The authors declare no competing interests.

**References**

Ardenkjær-Larsen, J.-H., Fridlund, B., Gram, A., Hansson, G., Hansson, L., Lerche, M. H., Servin, R., Thaning, M., and Golman, K.: Increase in signal-to-noise ratio of > 10,000 times in liquid-state NMR, Proc. Natl. Acad. Sci. U.S.A., 100, 10158-10163, https://doi.org/10.1073/pnas.1733835100, 2003.

Hirsch, M. L., Smith, B. A., Mattingly, M., Goloshevsky, A. G., Rosay, M., and Kempf, J. G.: Transport and imaging of brute-force (13)C hyperpolarization, J. Magn. Reson, 261, 87-94, https://doi.org/10.1016/j.jmr.2015.09.017, 2015.

Hirsch, M. L., Kalechofsky, N., Belzer, A., Rosay, M., and Kempf, J. G.: Brute-Force Hyperpolarization for NMR and MRI, J. Am. Chem. Soc., 137, 8428-8434, https://doi.org/10.1021/jacs.5b01252, 2015.

Ardenkjær-Larsen, J.-H.: On the present and future of dissolution-DNP, J. Magn. Reson., 264, 3-12, https://doi.org/10.1016/j.jmr.2016.01.015, 2016.

https://doi.org/10.5194/mr-2021-25
Preprint. Discussion started: 15 March 2021


Open Access MAGNETIC RESONANCE Discussions


Dale, M. W., and Wedge, C. J.: Optically generated hyperpolarization for sensitivity enhancement in solution-state NMR spectroscopy, Chem. Commun., 52, 13221-13224, https://doi.org/10.1039/C6CC06651H, 2016.

Barskiy, D. A., Coffey, A. M., Nikolaou, P., Mikaylov, D. M., Goodson, B. M., Brance, R. T., Lu, G. J., Shapiro, M. G., Telkki, V.-V., Zhivonitko, V. V., Koptyug, I. V., Salnikov, O. G., Kovtunov, K. V., Bukhtiyarov, V. I., Rosen, M. S., Barlow, M. J., Safavi, S., Hall, R. P., Schröder, L., and Chekmenev, E. Y.: NMR Hyperpolarization Techniques of Gases, Chem. Eur. J., 23, 724-724, https://doi.org/10.1002/chem.201604810, 2017.

Ardenkjær-Larsen, J.-H.: Introduction to Dissolution DNP: Overview, Instrumentation, and Human Applications, eMagRes, 7, 63-78, https://doi.org/10.1002/9780470034590.emrstm1549, 2018.

Kovtunov, K. V., Pokochueva, E. V., Salnikov, O. G., Cousin, S. F., Kurzbach, D., Vuichoud, B., Jannin, S., Chekmenev, E. Y., Goodson, B. M., Barskiy, D. A., and Koptyug, I. V.: Hyperpolarized NMR Spectroscopy: *d*-DNP, PHIP, and SABRE Techniques, Chem. Asian J., 13, 1857-1871, https://doi.org/10.1002/asia.201800551, 2018.

Meier, B.: Quantum-rotor-induced polarization, Magn. Reson. Chem., 56, 610-618, https://doi.org/10.1002/mrc.4725, 2018.

Jannin, S., and Kurzbach, D.: Dissolution Dynamic Nuclear Polarization Methodology and Instrumentation, eMagRes, 7, 117-132, https://doi.org/10.1002/9780470034590.emrstm1563, 2018.

Ardenkjær-Larsen, J.-H.: Hyperpolarized MR – What's up Doc?, J. Magn. Reson., 306, 124-127, https://doi.org/10.1016/j.jmr.2019.07.017, 2019.

Day, S. E., Kettunen, M. I., Gallagher, F. A., Hu, D.-E., Lerche, M., Wolber, J., Golman, K., Ardenkjær-Larsen, J.-H., and Brindle, K. M.: Detecting tumor response to treatment using hyperpolarized 13C magnetic resonance imaging and spectroscopy, Nat. Med., 13, 1382-1387, https://doi.org/10.1038/nm1650, 2007.

Brindle, K. M., Bohndiek, S. E., Gallagher, F. A., and Kettunen, M. I.: Tumor imaging using hyperpolarized 13C magnetic resonance spectroscopy, Magn. Reson. Med., 66, 505-519, https://doi.org/10.1002/mrm.22999, 2011.

Nelson, S. J., Kurhanewicz, J., Vigneron, D. B., Larson, P. E. Z., Harzstark, A. L., Ferrone, M., van Criekinge, M., Chang, J. W., Bok, R., Park, I., Reed, G., Carvajal, L., Small, E. J., Munster, P., Weinberg, V. K., Ardenkjær-Larsen, J.-H., Chen, A. P., Hurd, R. E., Odegardstuen, L.-I., Robb, F. J., Tropp, J., and Murray, J. A.: Metabolic imaging of patients with prostate cancer using hyperpolarized [1-$^{13}$C]pyruvate, Sci. Trans. Med., 5, 198ra108, https://doi.org/10.1126/scitranslmed.3006070, 2013.

Jannin, S., Dumez, J.-N., Giraudeau, P., and Kurzbach, D.: Application and methodology of dissolution dynamic nuclear polarization in physical, chemical and biological contexts, J. Magn. Reson., 305, 41-50, https://doi.org/10.1016/j.jmr.2019.06.001, 2019.

Kundu, K., Mentink-Vigier, F., Feintuch, A., and Vega, S.: DNP mechanisms, eMagRes, 8, 295-338, https://doi.org/10.1002/9780470034590.emrstm1550, 2019.

Meier, B., Dumez, J.-N., Stevanato, G., Hill-Cousins, J. T., Roy, S. S., Håkansson, P., Mamone, S., Brown, R. C. D., Pileio, G., and Levitt, M. H.: Long-Lived Nuclear Spin States in Methyl Groups and Quantum-Rotor-Induced Polarization, J. Am. Chem. Soc., 135, 18746-18749, https://doi.org/10.1021/ja410432f, 2013.

Roy, S. S., Dumez, J.-N., Stevanato, G., Meier, B., Hill-Cousins, J. T., Brown, R. C. D., Pileio, G., and Levitt, M. H.: Enhancement of quantum rotor NMR signals by frequency-selective pulses, J. Magn. Reson., 250, 25-28, https://doi.org/10.1016/j.jmr.2014.11.004, 2015.

Dumez, J.-N., Vuichoud, B., Mammoli, D., Bornet, A., Pinon, A. C., Stevanato, G., Meier, B., Bodenhausen, G., Jannin, S., and Levitt, M. H.: Dynamic Nuclear Polarization of Long-Lived Nuclear Spin States in Methyl Groups, J. Phys. Chem. Lett., 8, 3549-3555, https://doi.org/10.1021/acs.jpclett.7b01512, 2017.

Elliott, S. J., Meier, B., Vuichoud, B., Stevanato, G., Brown, L. J., Alonso-Valesueiro, J., Emsley, L., Jannin, S., and Levitt, M. H.: Hyperpolarized long-lived nuclear spin states in monodeuterated methyl groups, Phys. Chem. Chem. Phys., 20, 9755-9759, https://doi.org/10.1039/C8CP00253C, 2018.

Waugh, J. S., Gonen, O., and Kuhns, P.: Fourier transform NMR at low temperatures, J. Chem. Phys., 86, 3816-3818, https://doi.org/10.1063/1.451940, 1987.

Kuhns, P., Gonen, O., and Waugh, J. S.: Proton spin-spin and spin-lattice relaxation in CaSO4·x$H_2O$ below 1 K, J. Magn. Reson., 82, 231-237, https://doi.org/10.1016/0022-2364(89)90027-9, 1989.

Marohn, J. A., Carson, P. J., Hwang, J. Y., Miller, M. A., Shykind, D. N., and Weitekamp, D. P.: Optical Larmor beat detection of high-resolution nuclear magnetic resonance in a semiconductor heterostructure., Phys. Rev. Lett., 75, 1364-1367, https://doi.org/10.1103/PhysRevLett.75.1364, 1995.

Kuzma, N. N., Håkansson, P., Pourfathi, M., Ghosh, R. K., Kara, H., Kadlecek, S. K., Pileio, G., Levitt, M. H., and Rizi, R. R.: Lineshape-based polarimetry of dynamically-polarized $^{15}N_2O$ in solid-state mixtures, J. Magn. Reson., 234, 90-94, https://doi.org/10.1016/j.jmr.2013.06.008, 2013.

Mammoli, D., Salvi, N., Milani, J., Buratto, R., Bornet, A., Sehgal, A. A., Canet, E., Pelupessy, P., Carnevale, D., Jannin, S., and Bodenhausen, G.: Challenges in preparing, preserving and detecting para-water in bulk: overcoming proton exchange and other hurdles, Phys. Chem. Chem. Phys., 17, 26819-26827, https://doi.org/10.1039/C5CP03350K, 2015.

Willmering, M. M., Ma, Z. L., Jenkins, M. A., Conley, J. F., and Hayes, S. E.: Enhanced NMR with Optical Pumping Yields $^{75}$As Signals Selectively from a Buried GaAs Interface, J. Am. Chem. Soc., 139, 3930-3933, https://doi.org/10.1021/jacs.6b08970, 2017.

Aghelnejad, B., Marhabaie, S., Baudin, M., and Bodenhausen, G.: Spin Thermometry: A Straightforward Measure of Millikelvin Deuterium Spin Temperatures Achieved by Dynamic Nuclear Polarization, J. Phys. Chem. Lett., 11, 3219-3225, https://doi.org/10.1021/acs.jpclett.0c00713, 2020.

Ceillier, M., Cala, O., Chappuis, Q., Cousin, S. F., Elliott, S. J., and Jannin, S., *In Preparation*, **2021**.

Bornet, A., Milani, J., Vuichoud, B., Perez Linde, A. J., Bodenhausen, G., and Jannin, S.: Microwave frequency modulation to enhance Dissolution Dynamic Nuclear Polarization, Chem. Phys. Lett., 602, 63-67, https://doi.org/10.1016/j.cplett.2014.04.013, 2014.

Bornet, A., Pinon, A., Jhajharia, A., Baudin, M., Ji, X., Emsley, L., Bodenhausen, G., Ardenkjær-Larsen, J.-H., and Jannin, S.: Microwave-gated dynamic nuclear polarization, Phys. Chem. Chem. Phys., 18, 30530-30535, https://doi.org/10.1039/C6CP05587G, 2016.

https://doi.org/10.5194/mr-2021-25
Preprint. Discussion started: 15 March 2021


Open Access MAGNETIC RESONANCE Discussions

02 Latanowicz, L.: NMR relaxation study of methyl groups in solids from low to high temperatures, Concept Magn. Reson. A, 27A, 38-53,
03 https://doi.org/10.1002/cmr.a.20040, 2005.
04 Mao, X. A., and Ye, C. H.: Understanding radiation damping in a simple way, Concepts Magn. Reson. A, 9, 173-187, https://doi.org/10.1002/(SICI)1099-
05 0534(1997)9:3<173::AID-CMR4>3.0.CO;2-W, 1997.